



Letters

Process planning for hybrid manufacturing using additive friction stir deposition [☆]



Joshua Kincaid ^a, Elijah Charles ^a, Ryan Garcia ^a, Jake Dvorak ^a, Timothy No ^b, Scott Smith ^b, Tony Schmitz ^{a,b,*}

^a University of Tennessee, Knoxville, United States

^b Oak Ridge National Laboratory, United States

ARTICLE INFO

Article history:

Received 15 November 2022

Received in revised form 19 June 2023

Accepted 5 July 2023

Available online 17 July 2023

Keywords:

Additive friction stir deposition

Turning

Milling

Structured light scanning

ABSTRACT

Additive friction stir deposition (AFSD) provides a solid-state approach to metal deposition that does not rely on local melting and solidification, but rather on kinetic energy and plastic flow. In this study, AFSD is combined with structured light scanning, turning, and milling to produce metal components while considering the unique requirements imposed by the hybrid manufacturing process sequences. Two demonstrations are presented which include: 1) a cylindrical build plate selection to enable coordinate system transfer between deposition and turning of a hollow cone; and 2) intermittent deposition-machining operations with structured light scanning to fabricate a two-sided hexagon-cylinder geometry.

© 2023 Society of Manufacturing Engineers (SME). Published by Elsevier Ltd. All rights reserved.

1. Introduction

Beam-based metal additive manufacturing (AM) methods, including powder bed fusion and directed energy deposition, as well as wire arc AM, are finding broader applications in production. These methods melt the metal powder or wire using a high intensity heat source to deposit the material layer-by-layer. The geometry and microstructure are defined by the solidification behavior, which depends on the local temperature gradient and cooling rate [1]. Additive friction stir deposition (AFSD) provides a solid-state alternative [2–5], where no melting occurs and the geometry and microstructure are defined by the kinetic energy introduced by the AFSD process. Prior research has included the study of microstructure and its relationship to mechanical properties and operation parameters [6–15]. Materials include aluminum, magnesium, copper, and steel alloys [16–20]. Repair and cladding [21–

24], effect of alloy temper [25], fatigue behavior [26], process modeling [27], and force/temperature control [28] have also been examined.

In this paper, AFSD is combined with structured light scanning, turning, and milling to produce metal components while considering the hybrid manufacturing processes holistically to arrive at a comprehensive process plan. Deposition and machining strategies are presented for two geometries and materials. First, a 7075 aluminum cone is deposited and turned using a cylindrical build plate. Second, a 6061 aluminum hexagon-cylinder combination is deposited using a square build plate. Milling and turning are applied intermittently with deposition to enable part fabrication using both sides of the build plate. Structured light scanning is used to connect the deposition, machining, and part design coordinate systems in both cases [29–31].

In general, the hybrid manufacturing process plan includes seven primary steps: 1) digital part design; 2) path planning for AFSD; 3) metal deposition using AFSD to produce the preform; 4) measuring the preform to determine its geometry and identify its coordinate system using available (e.g., edge of the build plate) or added (e.g., tooling spheres) features, or fiducials; 5) path planning for CNC machining by importing the measured preform geometry and using it as the stock model with its predefined coordinate system; 6) CNC machining the preform to its design dimensions and surface finish using the coordinate system established by the fiducials; and 7) measuring the machined part to ensure conformance to design intent. These steps are summarized in Fig. 1.

[☆] This work was partially supported by the DOE Office of Energy Efficiency and Renewable Energy (EERE), Advanced Manufacturing Office (AMO), under contract DE-AC05-00OR22725. The US government retains the publisher, by accepting the article for publication, acknowledges that the US government retains a nonexclusive, paid-up, irrevocable, worldwide license to publish or reproduce the published form of this manuscript, or allow others to do so, for US government purposes. DOE will provide public access to these results of federally sponsored research in accordance with the DOE Public Access Plan (<https://energy.gov/downloads/doe-public-access-plan>).

* Corresponding author at: University of Tennessee, Knoxville, 114 Perkins Hall, Knoxville, TN 37902, United States.

E-mail address: tony.schmitz@utk.edu (T. Schmitz).

2. Manufacturing processes

AFSD was completed using a MELD Manufacturing L3 machine, which forces 9.5 mm square metal feedstock (e.g., wrought material) through a rotating spindle using a screw-type actuator located above the spindle. The actuator allows rotation of the 0.5 m long feedstock with the spindle while simultaneously providing the axial force and material feed against the build plate or previous layer. The feedstock rotation against the build plate/previous layer generates frictional heat, which softens the feedstock sufficiently to cause plastic flow and solid-state metallurgical bonding with the existing material. The printed material is constrained axially by the gap between the rotating tool and build plate/previous layer (1 mm to 3 mm). In the lateral direction, there is only friction between the plastically flowing material and the tool (on the top) and build plate/previous layer (on the bottom). For this reason, flash can occur at the outer portions of the current layer. The tool is translated parallel to the base plate/previous layer with a selected feed rate to print the current layer. Milling was completed using a Haas VF-4 three-axis CNC milling machine. Turning was completed using a Haas ST-15 CNC lathe. Structured light scanning was performed using a GOM ATOS Q.

3. Cone

The cone processing sequence included AFSD, scanning, turning, and surface finish measurements. The innovations were: 1) offset deposition paths to enable an angled (not vertical), hollow geometry; and 2) the selection of a cylindrical build plate to seamlessly combine the deposition and turning steps. The 25 mm thick, 216 mm diameter 7075 aluminum build plate was turned to final dimensions and then secured to the L3 table. This was accom-

plished by drilling and tapping blind holes in the back of the build plate, bolting it to a larger rectangular subplate using countersunk socket head cap screws, and clamping the subplate to the machine table using four toe clamps. The center of the cylinder was located using the L3 spindle and edge finder. The center of the build plate was set as the work coordinate system origin and the deposition tool paths were defined relative to the cone center. A helical interpolation scheme was used to deposit the 7075 aluminum bar stock. This alloy was selected because it is relevant to the aerospace (i.e., conical) geometry.

The 57.2 mm radius, 57.2 mm tall (45 deg) cone geometry is displayed in Fig. 2(a). For the 38 mm AFSD layer width, the initial tool path radius (at the build plate) was 63.5 mm to ensure that adequate material was available after flash removal by machining to achieve the design radius. Because the tool path radius was more than half the layer width, the cone base was hollow. A layer height of 1.5 mm was selected to define the helical interpolation tool path. The initial layer was deposited using a spindle speed of 300 rpm, material feed rate (through the spindle) of 58.4 mm/min, and tool feed rate (across the build plate surface) of 132.1 mm/min. Subsequent layers were deposited at 140 rpm with the same feed rates. The reduced spindle speed was applied due to heat buildup and increased temperature in the deposited material. The deposition is shown in Fig. 2(b), including the cylindrical build plate, subplate, and toe clamps.

After deposition, the build plate was released from the subplate and scanned to determine the deposition geometry. The scan result is shown in Fig. 2(c) and the superposition of the AM preform and cone design is displayed in Fig. 2(d). The scan origin was defined at the top center of the build plate. The design was then aligned at this same location.

Given the coincident origins, design geometry, and deposited material, the turning tool paths were generated by the CAM soft-

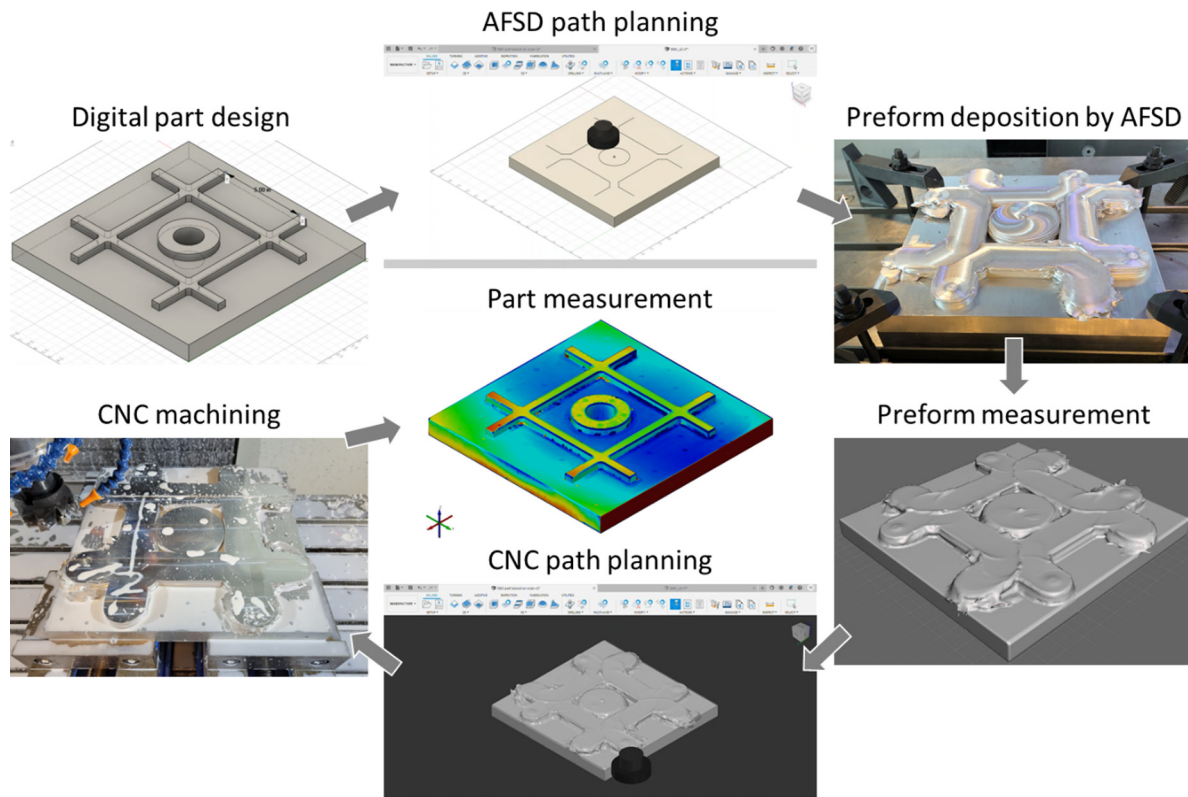


Fig. 1. Seven primary steps for hybrid manufacturing process plan beginning with digital part design and ending with part measurement [32].

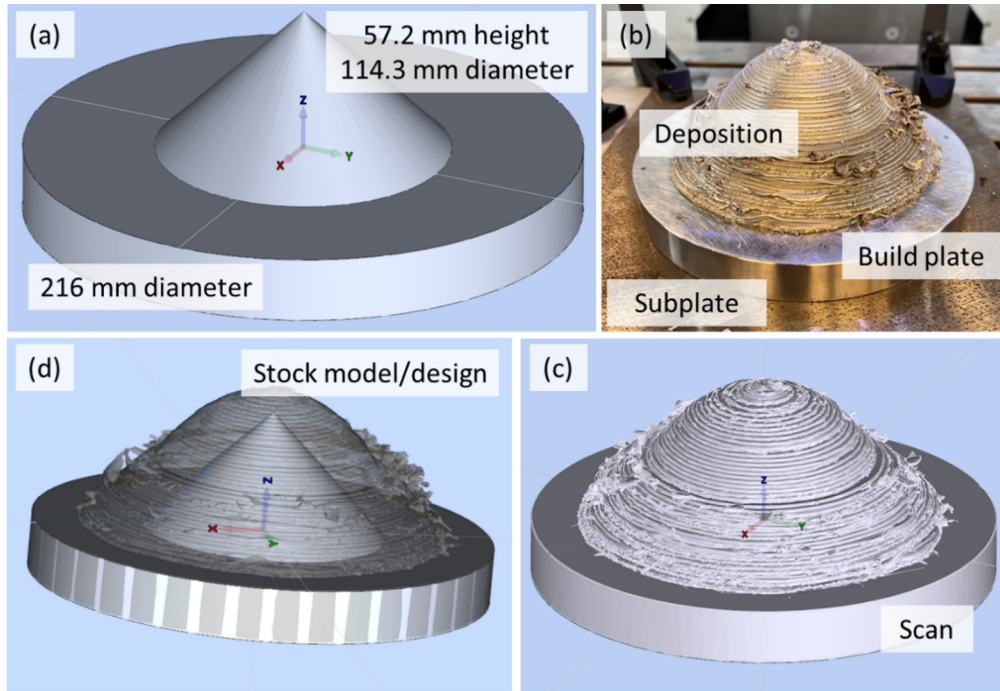


Fig. 2. A) Cone design. b) afsd deposition, build plate, and subplate. c) Scan result, including deposition and build plate. d) The scan serves as the CAM stock model. The center of the build plate from the scan and center of the cone base from the design are used to align the coordinate systems for tool path generation.

ware using the scan as the stock model. Because the tool paths were based on the cylinder top center, the only requirement for clamping in the CNC lathe was to provide three-jaw clamping surfaces that centered the part on the lathe spindle centerline. A single touch-off on the build plate surface in the lathe enabled the tool paths to be executed and the flash and extra deposited material to be removed and reveal the cone design.

The external soft jaw clamping approach is shown in Fig. 3(a). The cone geometry after rough turning is displayed in Fig. 3(b). The final cone is shown in Fig. 3(c). To reveal the hollow geometry, the cone was sectioned using wire electrical discharge machining (EDM). Fig. 3(d) shows the internal geometry. The additional material is flash that was developed on the internal edge of the helical deposit. The turning operation was completed using a 0.40 mm nose radius carbide insert with a 0.89 mm depth of cut, 243.8 m/min cutting speed, 0.13 mm/rev roughing feed rate, 0.05 mm/rev finishing feed rate, and flood coolant.

Surface finish measurements were completing near the cone tip using an Alicona 3D measuring system and Mitutoyo SJ-210 profilometer. Measurements were performed perpendicular to the feed direction at three equally spaced radial locations and averaged. Roughness values were 0.365 μm Ra for the Alicona and 0.369 μm Ra for the Mitutoyo.

4. Hexagon-cylinder

The hexagon-cylinder processing sequence included a two-sided 6061 aluminum deposition and intermittent machining approach. The hexagon was deposited first on a square 25 mm thick, 6061 aluminum build plate (the 6061 alloy was selected to demonstrate the ability to deposit both 7075 and 6061 aluminum alloys). The origin was set at the build plate top corner for the helical interpolation path planning to generate the hexagon shape using a 2 mm layer height. On the L3 machine, the spindle and edge finder were used to set the work coordinate system at the build plate top corner. Deposition then proceeded on the top sur-

face of the build plate, which was clamped to the machine table using four toe clamps (one at each corner). The initial layer was deposited using a spindle speed of 300 rpm, material feed rate of 139.7 mm/min, and tool feed rate of 132.1 mm/min. Subsequent layers were deposited at 160 rpm with the same feed rates.

After deposition, the hexagon preform and build plate were scanned. Fig. 4(a) displays the deposited hexagon. The part design and preform were then aligned using the origin at the build plate bottom corner and the milling tool paths were generated by CAM software with the imported scan used as the stock model; see Fig. 4(b). The build plate was clamped in a pair of pre-aligned vises on the CNC milling machine table. The machine probing cycle was used to set the work coordinate system at the build plate bottom corner and the milling tool paths were completed to produce the desired hexagon geometry; see Fig. 4(c). Finally, the hexagon was inverted and the extra build plate material was machined away to obtain the final hexagon dimensions; see Fig. 4(d). This inversion and machining step in a second vise setup motivated the location of the origin at the bottom of the build plate for the first setup. When turned over, the origin was located at the top of the part and could conveniently be identified using the machine probing cycle to set the new work coordinate system. Milling was completed using a spindle speed of 5115 rpm with a roughing feed rate of 3302 mm/min and finishing feed rate of 1397 mm/min. Flood coolant was applied.

Once the hexagon was complete, its base (i.e., the bottom of the original build plate) served as the build platform for the cylinder. The origin for the AFSD tool path planning was set at the center of the hexagon build plate surface, so this location was identified on the machine using the L3 spindle and edge finder. Deposition was completed using helical interpolation to generate the cylinder shape with a 2 mm layer height. The initial layer was deposited using a spindle speed of 275 rpm, material feed rate of 139.7 mm/min, and tool feed rate of 132.1 mm/min. Subsequent layers were deposited at 115 rpm with the same feed rates.

The cylinder preform is shown in Fig. 5(a) and the corresponding scan is provided in Fig. 5(b). By setting the scan (which served

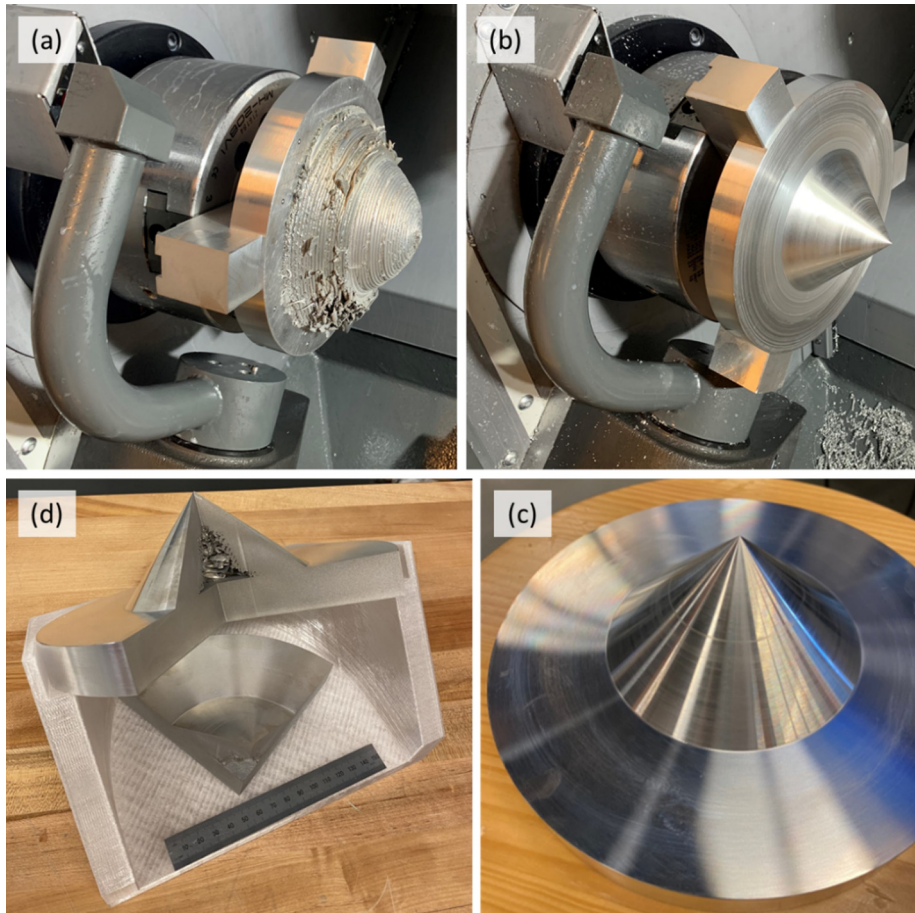


Fig. 3. A) Build plate and deposition clamped in lathe spindle. b) cone geometry after rough turning. c) finished cone. d) sectioned cone to show internal geometry. a 150 mm machinist's scale is included.

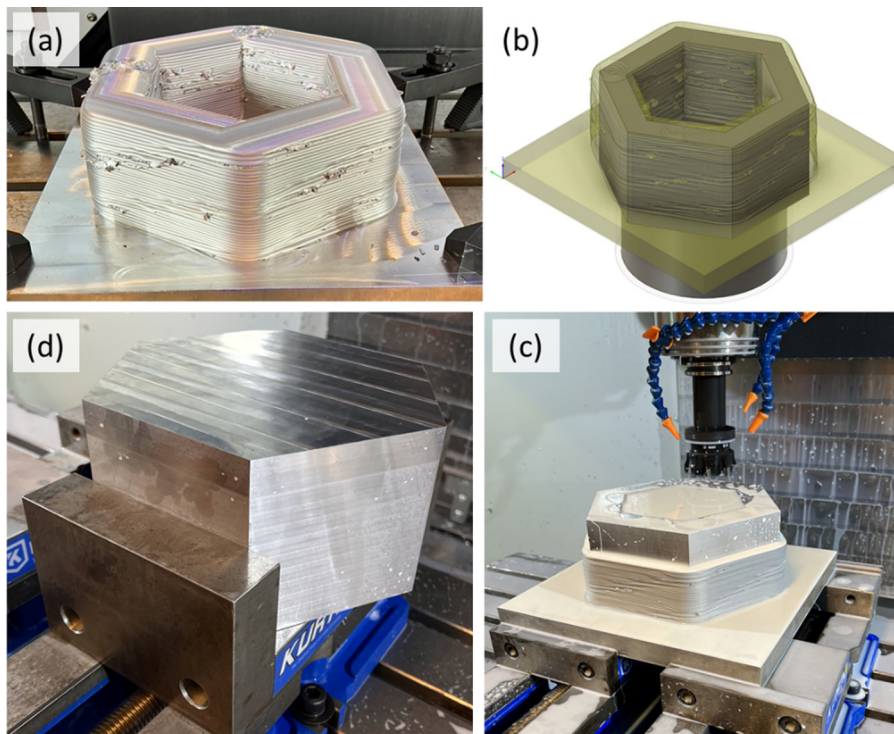


Fig. 4. A) Hexagon preform after a scan. b) Alignment of scan and part design. The origin for both coordinate systems is the build plate corner for convenient identification on the CNC milling machine using the probe. c) Milling the preform using a two-vise setup. d) Removing the build plate using a second vise setup where the part is inverted and clamped using opposing hexagonal surfaces. The same origin was maintained throughout the production sequence.

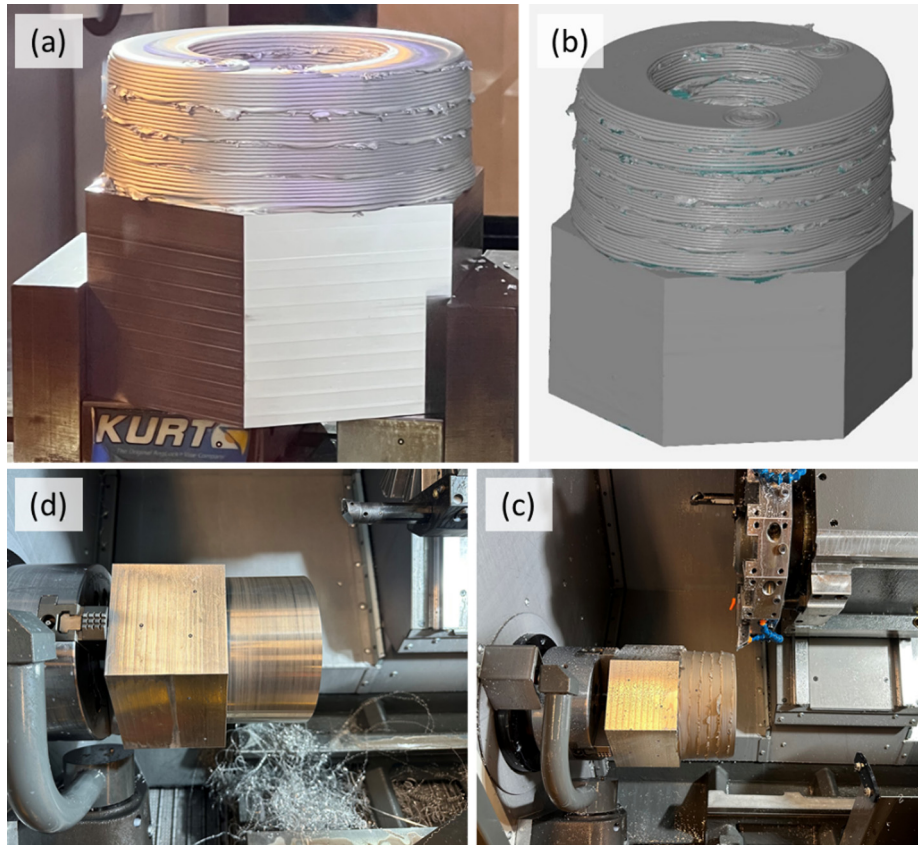


Fig. 5. A) Cylinder preform on hexagon base. b) scan of part after cylinder deposition. c) part clamped in lathe using three-jaw chuck on internal surfaces of hexagon. d) finished part before removal from lathe.

as the CAM stock model), design, and tool path coordinate systems at the center surface of the hexagon base, the lathe clamping requirement was simply to locate the part center on the spindle centerline. This was accomplished by using the lathe's three-jaw chuck to clamp three internal surfaces of the hexagon. This setup is shown in Fig. 5(c) and the finished part is displayed in Fig. 5 (d). The facing, turning, and boring operations were completed after touching off the hexagon base surface. The operating parameters were 243.84 m/min cutting speed, 0.89 mm, roughing depth of cut, 0.25 mm/rev roughing feed rate, 0.13 mm finishing depth of cut, 0.051 mm/rev finishing feed rate. The carbide insert nose radius 0.40 mm.

5. Conclusions

This paper demonstrated the combination of additive friction stir deposition (AFSD), turning, milling, and structured light scanning in a hybrid manufacturing scenario. Structured light scanning was used to generate stock models for tool path generation that incorporated coordinate systems that could be realized physically on the machining systems. The approach was shown by two selected part geometries. First, a cone geometry was selected to demonstrate AFSD for a hollow, non-vertical wall geometry and a cylindrical build plate was used to provide convenient coordinate system transfer and part clamping between the AFSD and turning processes. Second, a hexagon-cylinder geometry was fabricated using intermittent deposition and machining operations. The coordinate systems for the two-sided part (i.e., deposition was completed on both surfaces of the original build plate) were connected using structured light scanning and origins that could

be identified on the machining systems using standard probing routines. Both turning and milling operations were used to produce the final geometry and surface finish.

While microstructure and associated material properties of the deposited material were not the focus of this paper, these are important considerations for any additive manufacturing process, including AFSD. For the aluminum alloys studied in this paper, the strength and ductility depend on the deposition temperature. It has been shown that wrought-like material properties can be obtained for 7075 aluminum with appropriate solution treatment and peak aging [33]. These studies will be continued in parallel with the process planning efforts described here to arrive at an effective hybrid manufacturing approach.

Declaration of Competing Interest

The authors declare that they have no known competing financial interests or personal relationships that could have appeared to influence the work reported in this paper.

Acknowledgements

This work was partially supported by the DOE Office of Energy Efficiency and Renewable Energy (EERE), Advanced Manufacturing Office (AMO), under contract DE-AC05-00OR22725. The US government retains and the publisher, by accepting the article for publication, acknowledges that the US government retains a nonexclusive, paid-up, irrevocable, worldwide license to publish or reproduce the published form of this manuscript, or allow others to do so, for US government purposes. DOE will provide

public access to these results of federally sponsored research in accordance with the DOE Public Access Plan (<http://energy.gov/downloads/doe-public-access-plan>). The authors also acknowledge support from the DEVCOM Army Research Laboratory (grant no. W911NF2120020).

References

- [1] Dehoff RR, Kirka MM, Sames WJ, Bilheux H, Tremsin AS, Lowe LE, et al. Site specific control of crystallographic grain orientation through electron beam additive manufacturing. *Mater Sci Technol* 2015;31(8):931–8.
- [2] Hang ZY, Jones ME, Brady GW, Griffiths RJ, Garcia D, Rauch HA, et al. Non-beam-based metal additive manufacturing enabled by additive friction stir deposition. *Scripta Comput Sci Appl Math Materialia* 2018;153:122–30.
- [3] Khodabakhshi F, Gerlich AP. Potentials and strategies of solid-state additive friction-stir manufacturing technology: A critical review. *J Manuf Process* 2018;36:77–92.
- [4] Yu HZ, Mishra RS. Additive friction stir deposition: a deformation processing route to metal additive manufacturing. *Mater Res Lett* 2021;9(2):71–83.
- [5] Gopan V, Wins KLD, Surendran A. Innovative potential of additive friction stir deposition among current laser based metal additive manufacturing processes: A review. *CIRP J Manuf Sci Technol* 2021;32:228–48.
- [6] Priedeman JL, Phillips BJ, Lopez JJ, Tucker Roper BE, Hornbuckle BC, Darling KA, et al. Microstructure development in additive friction stir-deposited Cu. *Metals* 2020;10(11):1538.
- [7] Perry ME, Griffiths RJ, Garcia D, Sietins JM, Zhu Y, Hang ZY. Morphological and microstructural investigation of the non-planar interface formed in solid-state metal additive manufacturing by additive friction stir deposition. *Addit Manuf* 2020;35:101293.
- [8] Griffiths RJ, Garcia D, Song J, Vasudevan VK, Steiner MA, Cai W, et al. Solid-state additive manufacturing of aluminum and copper using additive friction stir deposition: Process-microstructure linkages. *Materialia* 2021;15:100967.
- [9] Agrawal P, Haridas RS, Yadav S, Thapliyal S, Gaddam S, Verma R, et al. Processing-structure-property correlation in additive friction stir deposited Ti-6Al-4V alloy from recycled metal chips. *Addit Manuf* 2021;47:102259.
- [10] Phillips BJ, Mason CJT, Beck SC, Avery DZ, Doherty KJ, Allison PG, et al. Effect of parallel deposition path and interface material flow on resulting microstructure and tensile behavior of Al-Mg-Si alloy fabricated by additive friction stir deposition. *J Mater Process Technol* 2021;295:117169.
- [11] Perry ME, Rauch HA, Griffiths RJ, Garcia D, Sietins JM, Zhu Y, et al. Tracing plastic deformation path and concurrent grain refinement during additive friction stir deposition. *Materialia* 2021;18:101159.
- [12] Williams MB, Robinson TW, Williamson CJ, Kinser RP, Ashmore NA, Allison PG, et al. Elucidating the effect of additive friction stir deposition on the resulting microstructure and mechanical properties of magnesium alloy we43. *Metals* 2021;11(11):1739.
- [13] Mukhopadhyay A, Saha P. A critical review on process metrics–microstructural evolution–process performance correlation in additive friction stir deposition (AFS-D). *J Braz Soc Mech Sci Eng* 2022;44(9):1–35.
- [14] Joshi SS, Sharma S, Radhakrishnan M, Pantawane MV, Patil SM, Jin Y, et al. A multi modal approach to microstructure evolution and mechanical response of additive friction stir deposited AZ31B Mg alloy. *Sci Rep* 2022;12(1):1–15.
- [15] Zeng C, Ghadimi H, Ding H, Nemati S, Garbie A, Raush J, et al. Microstructure Evolution of Al6061 Alloy Made by Additive Friction Stir Deposition. *Materials* 2022;15(10):3676.
- [16] Phillips BJ, Avery DZ, Liu T, Rodriguez OL, Mason CJT, Jordon JB, et al. Microstructure-deformation relationship of additive friction stir-deposition Al-Mg-Si. *Materialia* 2019;7:100387.
- [17] Alzahrani B, El-Sayed Seleman MM, Ahmed MM, Elfishawy E, Ahmed AM, Touileb K, et al. The Applicability of Die Cast A356 Alloy to Additive Friction Stir Deposition at Various Feeding Speeds. *Materials* 2021;14(20):6018.
- [18] Joshi SS, Patil SM, Mazumder S, Sharma S, Riley DA, Dowden S, et al. Additive friction stir deposition of AZ31B magnesium alloy. *J Magnesium Alloys* 2022.
- [19] Garcia D, Hartley WD, Rauch HA, Griffiths RJ, Wang R, Kong ZJ, et al. In situ investigation into temperature evolution and heat generation during additive friction stir deposition: A comparative study of Cu and Al-Mg-Si. *Addit Manuf* 2020;34:101386.
- [20] Beladi H, Farabi E, Hodgson PD, Barnett MR, Rohrer GS, Fabijanic D. Microstructure evolution of 316L stainless steel during solid-state additive friction stir deposition. *Philos Mag* 2022;102(7):618–33.
- [21] Griffiths RJ, Petersen DT, Garcia D, Yu HZ. Additive friction stir-enabled solid-state additive manufacturing for the repair of 7075 aluminum alloy. *Appl Sci* 2019;9(17):3486.
- [22] Hartley WD, Garcia D, Yoder JK, Poczatek E, Forsmark JH, Luckey SG, et al. Solid-state cladding on thin automotive sheet metals enabled by additive friction stir deposition. *J Mater Process Technol* 2021;291:117045.
- [23] Avery DZ, Cleek CE, Phillips BJ, Rekha MY, Kinser RP, Rao HM, et al. Evaluation of Microstructure and Mechanical Properties of Al-Zn-Mg-Cu Alloy Repaired via Additive Friction Stir Deposition. *J Eng Mater Technol* 2022;144(3):031003.
- [24] Peter Martin L, Luccitti A, Walluk M. Evaluation of Additive Friction Stir Deposition for the Repair of Cast Al-1.4 Si-1.1 Cu-1.5 Mg-2.1 Zn. *J Manuf Sci Eng* 2022;144(6).
- [25] Ahmed MM, El-Sayed Seleman MM, Elfishawy E, Alzahrani B, Touileb K, Habba MI. The effect of temper condition and feeding speed on the additive manufacturing of AA2011 parts using friction stir deposition. *Materials* 2021;14(21):6396.
- [26] Anderson-Wedge K, Avery DZ, Daniewicz SR, Sowards JW, Allison PG, Jordon JB, et al. Characterization of the fatigue behavior of additive friction stir-deposition AA2219. *Int J Fatigue* 2021;142:105951.
- [27] Stubblefield GG, Fraser K, Phillips BJ, Jordon JB, Allison PG. A meshfree computational framework for the numerical simulation of the solid-state additive manufacturing process, additive friction stir-deposition (AFS-D). *Mater Des* 2021;202:109514.
- [28] Merritt GR, Williams MB, Allison PG, Jordon JB, Rushing TW, Cousin CA. Closed-Loop Temperature and Force Control of Additive Friction Stir Deposition. *J Manuf Mater Process* 2022;6(5):92.
- [29] Dvorak J, Cornelius A, Corson G, Zamoski R, Jacobs L, Penney J, et al. A machining digital twin for hybrid manufacturing. *Manuf Lett* 2022;33:786–93.
- [30] Cornelius A, Jacobs L, Lamsey M, McNeil L, Hamel W, Schmitz T. Hybrid manufacturing of Invar mold for carbon fiber layup using structured light scanning. *Manuf Lett* 2022;33:133–42.
- [31] Cornelius A, Dvorak J, Jacobs L, Penney J, Schmitz T. Combination of structured light scanning and external fiducials for coordinate system transfer in hybrid manufacturing. *J Manuf Process* 2021;68:1824–36.
- [32] Kincaid J, Zamoski R, No T, Bohling J, Compton B, Schmitz T. Hybrid manufacturing: Combining additive friction stir deposition, metrology, and machining. *Friction Stir Welding and Processing XII*. In: Hovanski Y, Sato Y, Upadhyay P, Naumov AA, Kumar N, Editors. Part 1, The Minerals, Metals & Materials Society (TMS). Springer; 2023, ISBN 978-3-031-22660-1.
- [33] Yoder JK, Griffiths RJ, Hang ZY. Deformation-based additive manufacturing of 7075 aluminum with wrought-like mechanical properties. *Mater Des* 2021;198:109288.